JOURNAL OF MATERIALS SCIENCE 28 (1993) 4835–4840

High-resolution electron microscopy characterization of partially crystallized $Fe_{78}Si_{12}B_{10}$ alloy as a catalyst

L. WANG, G. W. QIAO, K. H. KUO
Laboratory of Atomic Imaging of Solids, Institute of Metal Research, Academia Sinica, Shenyang, 110015, People's Republic of China

Zh. J. CUI, K. Y. WANG
National Laboratory for Rapidly Solidified Nonequilibrium Alloys, Institute of Metal Research, Academia Sinica, Shenyang, 110015, People's Republic of China, China

As a catalyst, partially crystallized $Fe_{78}Si_{12}B_{10}$ alloy shows a three times higher activity than totally crystallized $Fe_{78}Si_{12}B_{10}$ in the hydrogenation of CO. High-resolution electron microscopy (HREM) reveals that the catalyst contains a great number of minute (less than 10 nm), highly dispersed α-Fe particles which act as the major active component. Many tiny B and Si oxide clusters also exist in the amorphous matrix. After being rinsed by a NaOH solution, the catalyst exhibits a decreasing selectivity to methane due to the dissolution or aggregation of B and Si species. After reaction, the sizes of the active particles increase and an overlayer of B or Si species is found over the surface of some α-Fe particles. This coverage is thought to be the primary origin of the deactivation of the catalyst.

1. Introduction

Over the past decades, efforts at searching for new types of catalysts have never been as plentiful as today. Amorphous materials, which differ greatly in electrical, magnetic and chemical properties from their crystalline counterparts, have been making a great impact on catalytic research. Since the first report of this kind in 1980 [1], increasing research has been carried out on the catalytic nature of amorphous materials and it has been found that under certain conditions most of the amorphous systems behaved better than the conventional catalysts in their activity, selectivity and stability. These systems include Zr-containing alloys (Ni–Zr, Fe–Zr) and Fe–(Ni)–B alloys. For example, in the hydrogenation of CO, which is a common test reaction for evaluating amorphous catalysts, $Ni_{63}Zr_{37}$ was found to achieve the optimal activity and selectivity of all the Fe-based and Ni-based Zr alloys [2]. Compared to the crystalline catalysts its Brunaver–Emett–Teller (BET) surface area was 50–70 times higher. In a Fe(Ni)–B(P) system [3], the increase in activity was more drastic. The value could be up to several hundred times higher than the crystalline samples.

In contrast to the increasing work on the reaction properties of the amorphous materials, little work has been carried out on their morphology, especially at the nanometre level. Scanning electron microscopy (SEM) is a usual method of revealing the rough surface of the catalysts [4–9]. Its resolution is at the micrometre level. But for the crucial morphological information, much higher resolution is needed since the characteristic active components are usually at the nanometre level. Scanning tunneling microscopy (STM) and high-resolution electron microscopy (HREM) are the proper techniques for this purpose. There have been some STM temptations in recent years. For example, in 1988 Walz *et al.* gave a report on a FeZr system [10] in which they identified surface similarities between the amorphous and the reacted samples and concluded that the surface of the as-received amorphous alloy was at least partially crystallized. For HREM, it is a little more difficult to find practical applications due to a number of problems, e.g. radiation instability of samples, disturbance of the substrate to the active phase when in imaging, etc. But advances have been obtained recently, and HREM has proved a valuable technique in the catalysis field [11, 12]. For amorphous materials, the advantage of HREM is more obvious because of its phase-contrast imaging. And the short-range ordering of even tiny crystalline nuclei, which are often present in metallic glasses and cannot be easily seen by conventional transmission electron microscopy (TEM), can be clearly and directly disclosed by HREM. A few examples in this field have been reported, such as the report by Trudeau *et al.* at the Seventh International Conference on Rapidly Quenched Materials. Their results for a ball-milled Ni–Mo system clearly indicated that a large quantity of small Ni, Mo crystallites

Please send correspondence to: Dr Long Wang, Department of Materials Science and Engineering, Case Western Reserve University, Cleveland, OH 44106, USA.

0022–2461

existed in an amorphous matrix. After about 10 or 15 h of milling, many dislocations were produced in the crystals. When the size of crystallites was less than 10 nm, all the dislocations vanished. They also claimed that the long milling time produced high-angle grain boundaries and that further analysis was on the way.

Fe–Si–B systems are a typical metallic glass which has attracted many researchers in recent years. The activity measurements on $Fe_{78}Si_{12}B_{10}$ showed that the value of the partially crystallized sample is three times higher than that of the crystalline sample [13]. In order to understand its chemical behaviour, we initiated a systematic HREM investigation of this system and found that a great number of α-Fe fine particles, some iron-oxide particles and B or Si species clusters were present in the amorphous matrix. In addition, the influences on the selectivity and deactivation are discussed on the basis of the observed results.

2. Experimental procedure

The $Fe_{78}Si_{12}B_{10}$ alloys were prepared first, by a melt-spinning technique to generate ribbons about 5 mm wide and 25–30 μm thick; then they were annealed carefully in an argon atmosphere below the crystallization temperature. The annealing treatment introduces some crystallinity into the catalyst and is thought by many reporters as an important way of activating the catalyst [2, 14–19]. In order to obtain a larger specific surface, a planetary ball mill was used to grind the ribbons in the presence of an alcohol solution, preventing possible contamination. As a comparison, a totally annealed sample (sample B) and the original casting sample (sample C) were also tested. Fig. 1 is an X-ray diffraction (XRD) pattern of the three samples. In the measurement of the activities, the catalysts were taken into a flow microreactor and subjected to the hydrogenation of CO. Fig. 2 is the activity measurement of the three samples. One can see that activity of the partially crystallized sample (sample A) is three times higher than that of the totally crystallized sample, and six times higher than that of the original casting sample. To investigate the selectivity behaviour, the partially crystallized sample was subjected to a rinsing treatment with a NaOH solution. This rinsing resulted in a considerable decrease (72 to 40%) in selectivity to methane [13]. In this paper, the major HREM work concentrates on the partially crystallized sample (sample A). Table I lists the treatment for all the samples.

The samples for HREM were made by a conventional powder technique as follows: the powders were first ground in an agate mortar which contained non-aqueous alcohol, then were collected on a holed carbon film on a copper grid. All the observations were carried out on a JEOL-200CX microscope with a point resolution of 0.25 nm.

3. Results and discussion

3.1. Partially crystallized $Fe_{78}Si_{12}B_{10}$

Fig. 3 shows the morphology of the $Fe_{78}Si_{12}B_{10}$ at low magnification and its diffraction pattern before reaction. In the diffraction pattern, all the rings except the innermost ring correspond to α-Fe and a portion of the {1 1 0} ring was used to form a dark-field image (Fig. 3a). From Fig. 3 one can see that the catalyst is composed of numerous fine α-Fe particles which are highly dispersed in the amorphous matrix, with irregular shapes and sizes less than 10 nm. They are the major crystalline phase in the catalyst, and the result is consistent with the XRD result (Fig. 1 curve A). It is easily understood that these small crystallites were

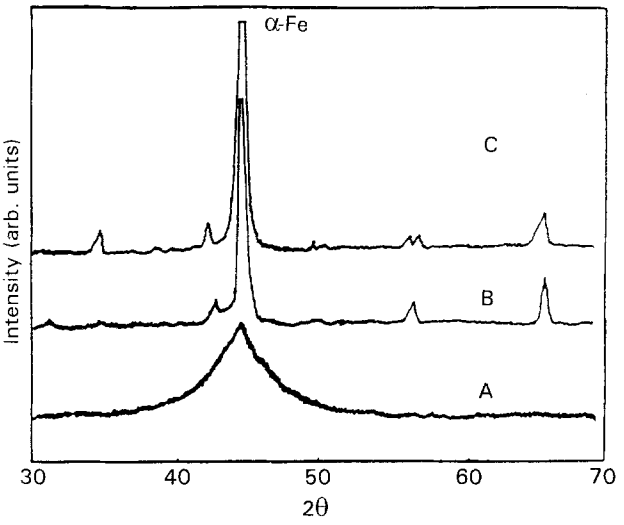

Figure 1 XRD pattern of catalysts A, B, C (CuK_α).

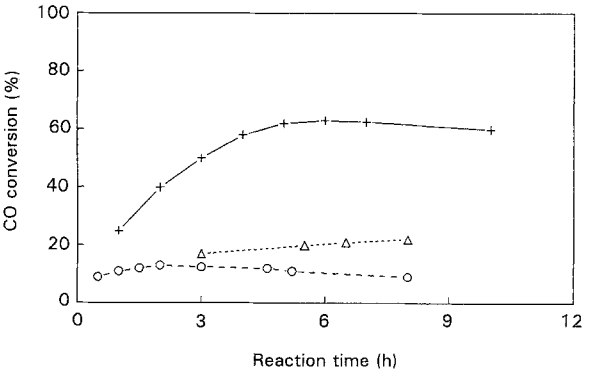

Figure 2 Activity curve of the three samples: (— + —) A, (- - -△- - -) sample B, and (- - -O- - -) sample C.

TABLE I The composition, preparation and related states of the three catalyst samples

Catalyst	Composition	Preparation	State
A	$Fe_{78}Si_{12}B_{10}$	Ball milled, partially crystallized	Almost amorphous
B	$Fe_{78}Si_{12}B_{10}$	Ball milled, totally crystallized	Microcrystalline
C	$Fe_{78}Si_{12}B_{10}$	Ball milled, crystallized casting	Polycrystalline

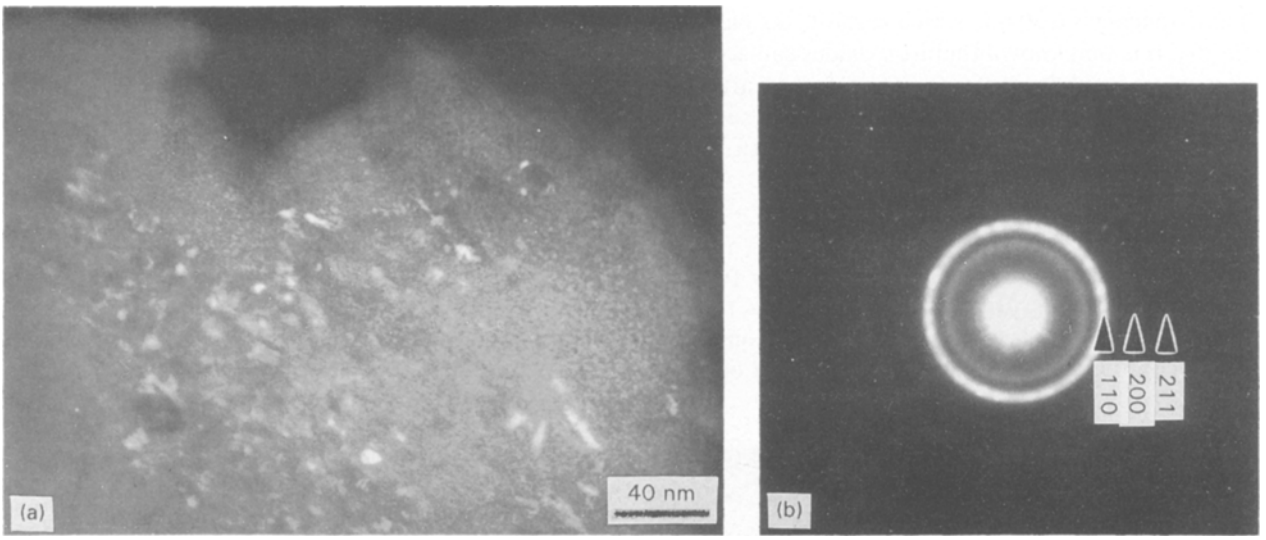

Figure 3 (a) Dark-field morphology and (b) electron-diffraction pattern of the partially amorphous $Fe_{78}Si_{12}B_{10}$ sample.

introduced by controlled annealing since the as-received sample was totally amorphous. Fig. 4 shows a high resolution image of one of the α-Fe particles. The lattice spacing corresponds to α-Fe {1 1 0} planes. Due to the disturbance of the thick amorphous matrix, the edge of the particle is not clear. But we still can measure the size of the particle by counting the numbers of the planes. It is about 8 nm. By comparing the activity and the XRD curves of the three samples A, B, C, the major decrease in size of the α-Fe particles is responsible for the activity change. Although the catalytic mechanism in the amorphous catalyst is still unclear, it has been thought that the existence of the crystallinity in the amorphous matrix is essential to its catalytic properties [20], and addition of a controlled amount of crystallinity, therefore, not only helps by activating the catalyst, but it also extends the active sites.

Except for the major active phase of α-Fe particles, some other species were found in the catalyst. Note the innermost ring in Fig. 3b has a *d*-spacing of 0.26 nm and does not belong to the α-Fe. The dark-field image did not reveal much information about it due to its weak intensity and due to the disturbance of the matrix. The high-resolution image indicates that it is mainly from the contribution of small clusters in the matrix (Fig. 5). They are too small (< 5 nm) to be identified by XRD. We suggest that these small clusters are non-iron-oxide species, e.g. B_2O_3, SiO_2 since the oxygen was readily introduced when the sample was exposed to air (although the iron oxides can also make a contribution to the 0.26 nm diffraction ring, they are supposed to be large in size and have better contrast in such images, as discussed later). These tiny clusters are widely distributed in the matrix, forming a chemical surrounding of the α-Fe particles. The interaction between them has been discussed in some reports [21, 22] and it is suggested that the aggregation of boron as an oxide on the surface can promote nucleation of the α-Fe from the matrix during reaction and also suppress its over-growth. The sizes of the α-Fe particles can be controlled by the boron oxide as optimum for activity.

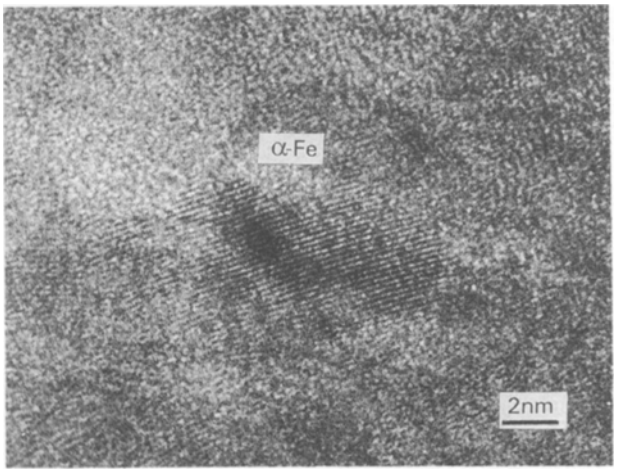

Figure 4 High-resolution image of an α-Fe particle in a partially amorphous sample.

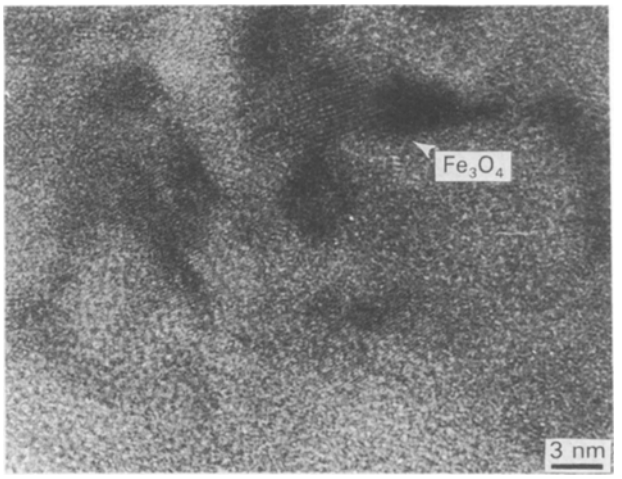

Figure 5 High-resolution image of the minute non-iron particles in the amorphous matrix.

Since the sample was exposed to air, some Fe oxides were expected to exist in the catalyst. Fig. 6 shows one of the iron-oxide particles. The image contrast is better than the tiny clusters because of its larger size (> 10 nm) and higher atomic-scattering factor.

The *d*-spacing is 0.30 nm, which suggests the particle is Fe_3O_4. It is well known that iron oxides can act as the precursors in hydrogenation, because they are easily reduced in H_2 atmospheres. Hence they are supposed to make a minor contribution to the activity.

3.2. Rinsed $Fe_{78}Si_{12}B_{10}$

After being rinsed by a NaOH solution, the partially crystallized $Fe_{78}Si_{12}B_{10}$ catalyst showed a remarkable decrease in selectivity to methane (from 72 to 40%). In structure, the major change did not occur on the α-Fe particles, but instead it occurs in the matrix. Rinsing treatment is a significant way of improving the surface status of the active component as well as the matrix. They could not, of course, change the sizes of the α-Fe particles. In the rinsing solution, boron and silicon were detected by emission microscopy. This means that the boron or silicon species in the matrix reacted with NaOH, making themselves either dissolve or aggregate together to form large crystal precipitates. High-resolution micrographs reveal that some residual B_2O_3 precipitates still remain on the matrix. They are in strips, which can be 150 nm long and 10 nm wide (Fig. 7). So, due to the NaOH rinsing, the composition of the matrix changed and the chemical circumstances surrounding the α-Fe particles changed from acidic to neutral, or even alkaline. This effect is equal to an addition of an electronic promotor into the catalyst, which favours the hydrogenation of CO in Fischer–Tropsch (F–T) synthesis. By their selectivity, the final products, therefore, contain smaller amounts of methane and more high-carbon-number F–T products.

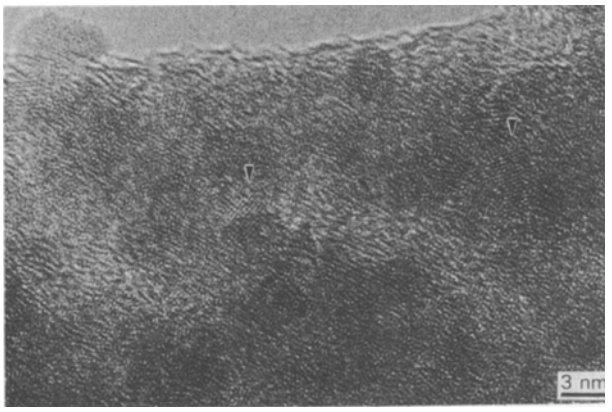

Figure 6 High-resolution image of an Fe_3O_4 particle in the partially amorphous sample.

3.3. The reacted $Fe_{78}Si_{12}B_{10}$

After reacting for about 10 h, the amorphous catalyst began to show a lower activity (Fig. 2). Growth of the α-Fe particle can be found. Fig. 8 is a dark-field micrograph of the reacted particles. Their sizes have

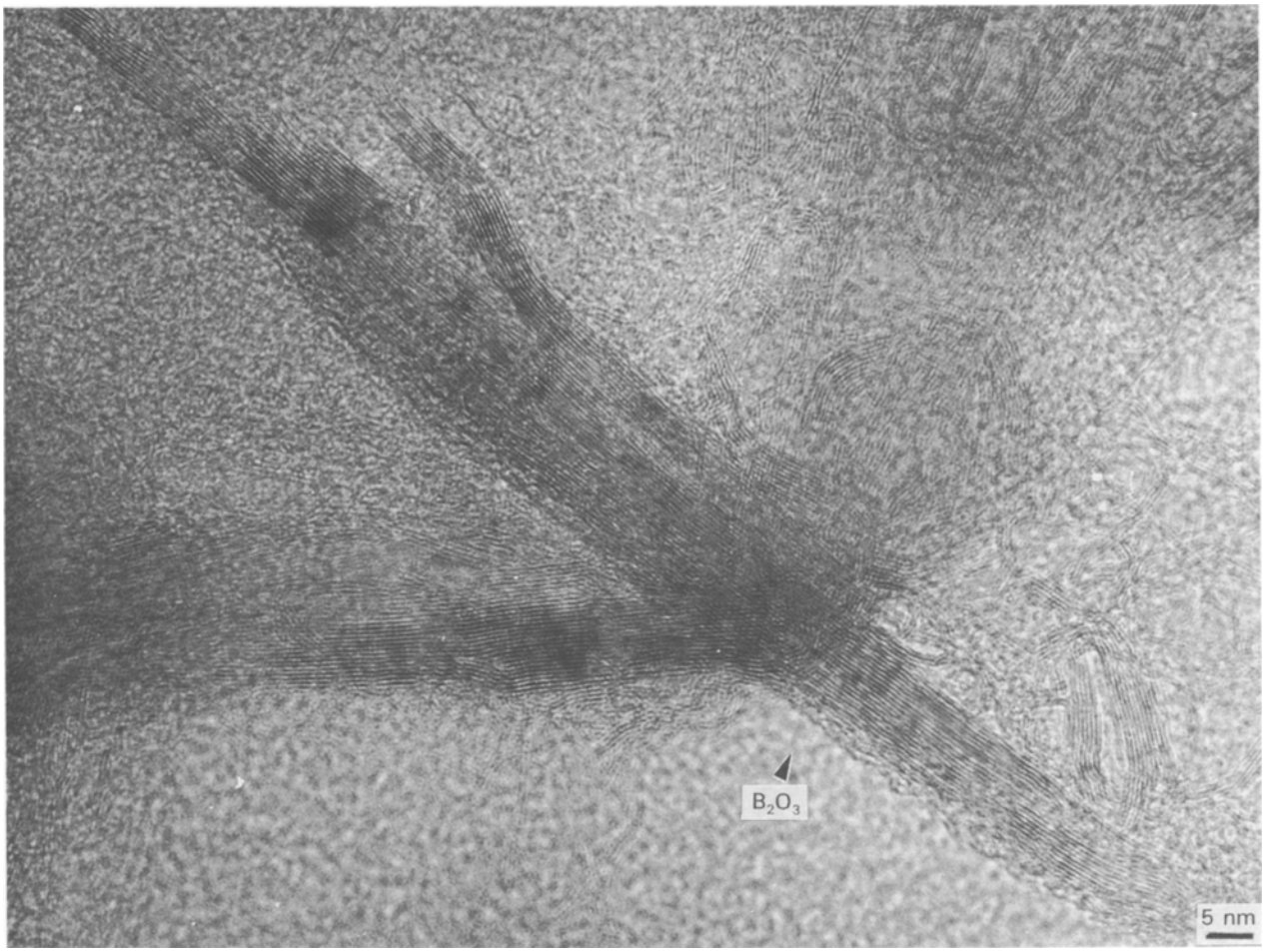

Figure 7 High-resolution image of some B_2O_3 strips after the NaOH treatment.

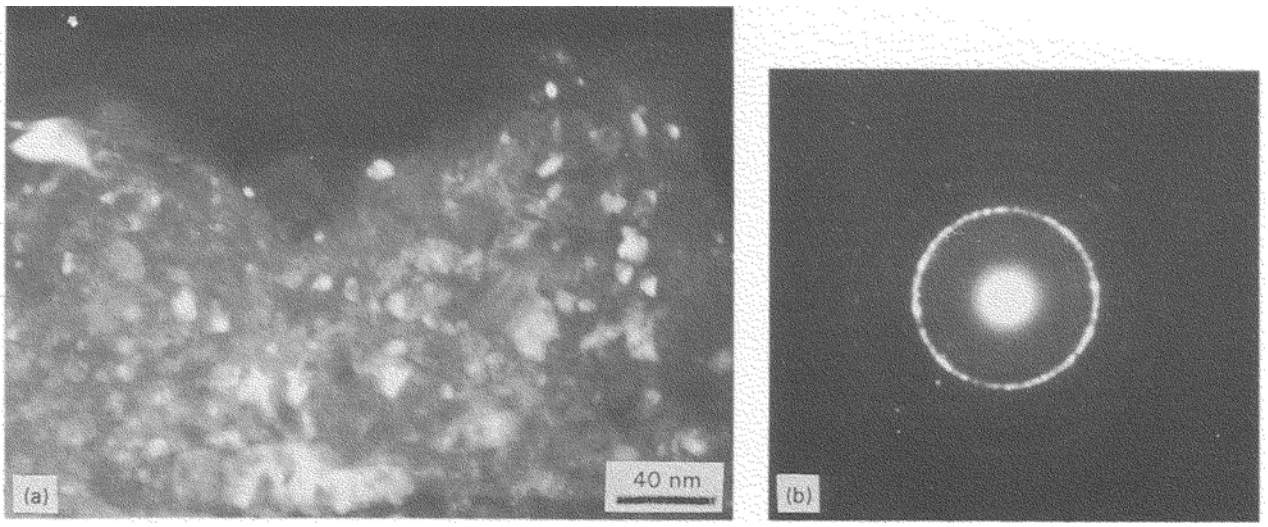

Figure 8 (a) Dark-field morphology and (b) diffraction pattern of reacted, partially amorphous $Fe_{78}Si_{12}B_{10}$.

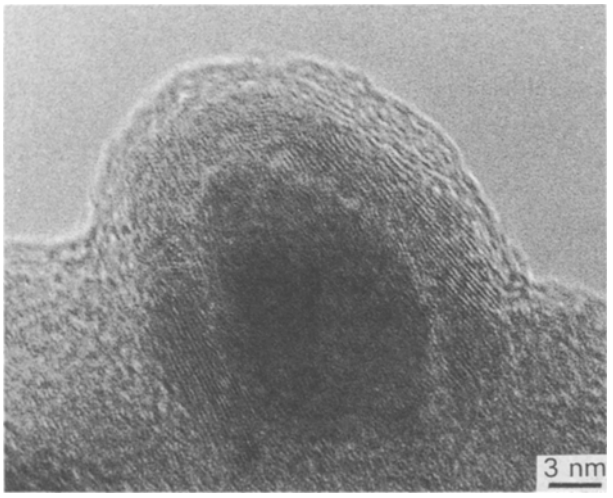

Figure 9 A metal particle with a B or Si species overlayer on its surface in reacted, partially amorphous $Fe_{78}Si_{12}B_{10}$.

increased to 10–30 nm. This kind of deactivation caused by size increase is usually referred to sintering. However, we found that a coking effect might also be responsible for the loss of the activity. In F–T synthesis, the coking deposits are often carbon species. But in our case, the deposit is something different from a carbon species. As the high-resolution image reveals in Fig. 9, the particle was covered by an overlayer which showed one-dimensional lattice fringes. Its *d*-spacing is the same as that of the innermost ring in Fig. 3b, implying that the deposit is more likely to be an oxide of B or Si than a carbon species, which would otherwise display an amorphous feature. This B- or Si-oxide overlayer surely comes from the matrix during reaction. It is premature to predict the migration mechanism on the basis of only the above results. But one can visualize that this coking effect would be more severe than sintering and might be the final cause of the total poisoning of the catalyst.

4. Conclusion

HREM has been used to characterize a partially crystallized $Fe_{78}Si_{12}B_{10}$ system that shows a three times higher activity than the totally crystallized system in the hydrogenation of CO. The observations reveal that a great number of minute (less than 10 nm), highly dispersed α-Fe particles are the major active components of the catalyst. In the amorphous matrix, many tiny B or Si clusters or their oxide clusters also exist. After being rinsed by a NaOH solution, the catalyst showed a decreasing selectivity to methane due to the dissolution or aggregation of boron or silicon species. In the reacted catalyst, we found that the sizes of the particles increased, and an overlayer of B or Si species arose over the surface of some α-Fe particles. This coverage is suggested to be the primary origin of the deactivation of the catalyst.

References

1. G. V. SMITH, W. E. BROWER, M. S. MATYJASZCZYK and T. L. PETTIT, in Proceedings of the Seventh International Congress on Catalysis, Tokyo (1980) p. 355.
2. A. YOKOYAMA, H. KOMIYAMA, H. INOUE, T. MASUMOTO and H. KIMURA, *Shokubai A* **9** (24) (1982) 61.
3. A. YOKOYAMA, H. KOMIYAMA, H. INOUE, T. MASUMOTO and H. KIMURA, *J. Catalysis* **68** (1981) 355.
4. H. YAMASHITA, M. YOSHIKAMA, T. KAMINADE, T. FUNABIKI and S. YOSHIDA, *J. C. S., Faraday I* **82** (1986) 207.
5. M. ENYO, T. YAMAZAKI, K. KAI and K. SUZUKI, *Electrochim. Acta* **28** (1983) 1573.
6. K. MACHIDA, M. ENYO, I. TOYISHIMA, K. KAI and K. SUZUKI, *J. Less-Common Metals* **96** (1984) 305.
7. K. MACHIDA, M. ENYO, K. KAI and K. SUZUKI, *J. Less-Common Metals* **100** (1984) 377.
8. A. KAWASHIMA and K. HASHIMOTO, in Proceedings of the Fourth International Conference on Rapidly Quenched Materials, (Sendai, 1981) p. 1427.
9. A. KAWASHIMA and K. HASHIMOTO, *Sci. Rep. RITU A* **31** (1983) 174.
10. B. WALZ, R. WIESENDANGER, L. ROSENTHALER, H. J. GUNTHERODT, M. DUGGELIN and R. GUGGENHEIM, *Mater. Sci. Engng* **99** (1988) 501.
11. J. M. THOMAS, G. R. MILLARD, S. ROMDAS, L.A. BURSILL and M. AUDIER, *Faraday Discuss. Chem. Soc.* **72** (1981) 345.
12. L. WANG, G. W. QIAO, H. Q. YE, K. H. KUO and Y. X. CHEN, in Proceedings of the Ninth International Congress on Catalysis **3** (1988) p. 1253.

13. Zh. J. CUI, L. WANG, K. Y. WANG, Q. H. SONG, J. T. WANG and K. LU *Mater. Sci. Engng A* **134** (1991) 1037.
14. M. SHIBATA, Y. OHBAYASHI, N. KAWATA, T. MASUMOTO and K. AKI, *J. Catal.* **96** (1985) 296.
15. M. SHIBATA, N. KAWATA, T. MASUMOTO, H. KIMURA and S. KIMITSU, *Chem. Lett.* (1985) 1605.
16. A. YOKOYAMA, H. KOMIYAMA, H. INOUE, T. MASUMOTO and H. KIMURA, *Chem. Lett.* (1983) 195.
17. A. YOKOYAMA, H. KOMIYAMA, H. INOUE, T. MASUMOTO and H. KIMURA, *J. Non-Cryst. Solids*, **61/62** (1984) 619.
18. Y. SHIMOGAKI, H. KOMIYAMA, H. INOUE, T. MASUMOTO and H. KIMURA, *Chem. Lett.* (1985) 661.
19. L. GUCZI, Z. ZSOLDOS and Z. SCKAY, *J. Vac. Sci. Technol. A* **5** (1987) 1070.
20. U. KOSTER, *Z. Metallkde* **75** (1984) 691.
21. K. ASAMI, H. KIMURA, K. HASHIMOTO and T. MASUMOTO, *J. Non-Cryst. Solids* **64** (1984) 135.
22. K. ASAMI, H. KIMURA, K. HASHIMOTO, T. MASUMOTO, A. YOKOYAMA, H. KOMIYAMA and H. INOUE, *J. Non-Cryst. Solids* **64** (1984) 149.

Received 27 April 1992
and accepted 24 February 1993